Materials and Design 107 (2016) 153–162

Contents lists available at ScienceDirect

Materials and Design

journal homepage: www.elsevier.com/locate/matdes

Gaining flexibility in the design of microstructure, texture and shape memory properties of an Fe-Mn-Si-Cr-Ni alloy processed by ECAE and annealing

A.V. Druker [a,b,*], A. Baruj [c,d,e], L. Isola [a,b], V. Fuster [a,b], J. Malarría [a,b], R. Bolmaro [a,b]

[a] Instituto de Física Rosario (CONICET-UNR), Bv. 27 de Febrero 210 bis, 2000 Rosario, Argentina
[b] Facultad de Cs. Ex., Ingeniería y Agrimensura (UNR), Av. Pellegrini 250, 2000 Rosario, Argentina
[c] Centro Atómico Bariloche, Comisión Nacional de Energía Atómica (CNEA), Av. Ezequiel Bustillo 9500, 8400 S. C. de Bariloche, Argentina
[d] Instituto Balseiro (UNCuyo), Av. Ezequiel Bustillo 9500, 8400 S. C. de Bariloche, Argentina
[e] CONICET, Argentina

ARTICLE INFO

Article history:
Received 4 March 2016
Received in revised form 6 June 2016
Accepted 9 June 2016
Available online 10 June 2016

Keywords:
Ferrous shape memory alloys
ECAE
Martensitic transformation
Microstructure
X-ray diffraction

ABSTRACT

The effect of ECAE on the properties of an Fe-15Mn-5Si-9Cr-5Ni shape memory alloy (SMA) was investigated. Phases, texture, microstructure, critical temperatures, mechanical and SM properties after severe deformation, and the effect of annealing were analysed. One ECAE pass develops a shear texture. There is a large ⟨101⟩ component in the extrusion direction, which is near the ideal ⟨414⟩ for martensitic transformation activation. The pressing did not refine the previous as cast structure but introduced dislocations and ε-martensite. Thus, the stress to induce the $\gamma \rightarrow \varepsilon$ martensitic transformation, $\sigma_{\gamma \rightarrow \varepsilon}$, reached 620 MPa, and the quantity of ε-martensite formed after compression was limited. The degree of shape recovery was reduced, while the reverse transformation temperatures increased. Heat treatments above 800 °C activated recrystallization. As annealing temperature increased, new grains nucleated and grew, reaching a size of 53 μm after heating to 1000 °C. For this condition, $\sigma_{\gamma \rightarrow \varepsilon}$ was 430 MPa, and the best shape recovery was achieved, 64%.

1. Introduction

The study of FeMnSi SMAs is a very interesting field of research due to the material's wide spread application, for example in easily assembled/low-cost couplings. Its particular shape memory effect (SME) results from a reversible, stress-induced, γ (austenite, FCC) ↔ ε (martensite, HCP) martensitic transformation, with a reverse transformation which activates when the material is heated to an appropriate temperature. The stacking fault energy (SFE) of these alloys is lower than 20 mJ/m^2. Thus, perfect dislocations dissociate into two Shockley partial dislocations, and the $\gamma \rightarrow \varepsilon$ martensitic transformation can occur by the movement of these partials. This depends on crystal orientation. In the early 1980s [1], studies of single crystals showed that the $\gamma \rightarrow \varepsilon$ martensitic transformation is nearly absent if a stress acts in the [001] direction and almost perfect when it acts along the [414] direction. By extension, certain crystallographic textures in polycrystals will contribute to a better shape recovery at lower applied stresses.

In a previous work [2], we investigated the effect of texture on the SME. After rolling at room temperature, we obtained a relatively strong ⟨101⟩ component at ~30° to the rolling direction, which is characteristic of FCC rolling textures. The anti-symmetrical component of the velocity gradient in a shearing process tends to reorient, albeit with decreasing intensity, the usual rolling-texture components. On the other hand, we found that hot-rolled samples contained a ⟨101⟩ component parallel to the rolling direction (⟨101⟩//RD) up to a certain depth into the sheet. This component vanishes after tensile deformation. In grains with an ideal orientation (the ⟨414⟩ directions lie parallel to the tensile axis) a selective motion of Shockley partial dislocations on the {111}⟨112⟩ system occurs. This leads to a depletion of the ⟨414⟩ component due to the $\gamma \rightarrow \varepsilon$ martensitic transformation. In our rolling study, the beneficial shearing component was almost absent at greater depths, and most probable was only induced on the surface due to a high frictional interaction between the rolls and work piece at elevated temperature.

Because of the limitations encountered in hot rolling, in this study we turned to the Equal-Channel Angular Extrusion (ECAE) process [3] in order to obtain a strong ⟨101⟩//RD component. ECAE produces a shear texture due to the spin imposed by the shearing process. This method is well known due to the interest in ultrafine grain and nanostructured materials. Fine grain sizes can be achieved by passing a billet many times through an extrusion channel, like shown in Fig. 1a. Previously, W. Zhang et al. [4–6] obtained an improved SME in an Fe-19.04Mn–4.98Si–8.50Cr–4.59Ni-(0.013C) alloy through ECAP. More

* Corresponding author at: Instituto de Física Rosario (CONICET-UNR), Bv. 27 de Febrero 210 bis, 2000 Rosario, Argentina.
E-mail address: druker@ifir-conicet.gov.ar (A.V. Druker).

http://dx.doi.org/10.1016/j.matdes.2016.06.036
0264-1275/

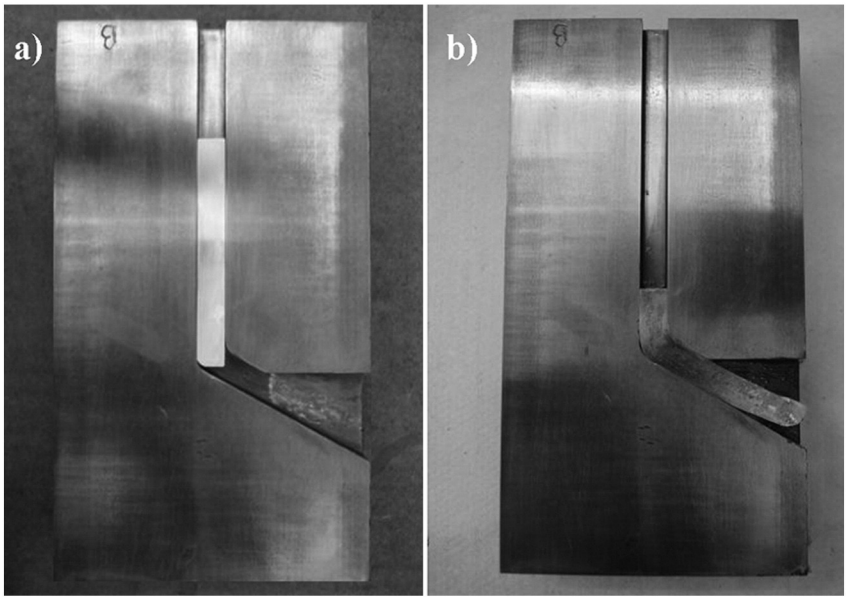

Fig. 1. (a) The ECAE block prepared for extrusion (b) The block after the deformation was interrupted.

recently, Bernardi et al. [7] investigated the shape recovery in a Fe-14.2Mn-5.3Si-8.8Cr-4.65Ni alloy with and without Co, after deformation by ECAE. They also observed an enhanced SME after processing, attributing their results to grain refinement effects without considering that ECAE also affects the texture [8–12]. In fact, grain refinement might degrade the SME. In 2012, we studied ribbons of an ultra-fine grain size Fe-Mn-Si alloy. The ribbons, produced by rapid solidification, exhibited no satisfactory degree of shape recovery (DSR) [13]. First, when grain size decreases, the SFE increases [14]. In addition, in small grains the martensite tip can easily reach the boundary, forcing large strain fields to build up and relax by irreversible slip. Other options, such as formation of alternative variants, are restricted by the constraint imposed by the grain boundary. Moreover, due to the low symmetry change of its martensitic transformation the Fe-Mn-Si based alloy is considerably limited in its ability to accommodate strains through other variants [15]. So, a mismatch at grain boundaries and other sites where high strain fields are produced is resolved by slip. Recently, Wang et al. [16] also found that grain refinement suppresses the stress-induced ε martensitic transformation.

Thus, this work investigates how severe deformation can affect the properties of an Fe-15Mn-5Si-9Cr-5Ni SMA. The possible reorientation of the main rolling components to a texture where the ⟨110⟩ directions lie along the Extrusion Direction (ED) was of particular interest. We also investigated whether the high energy accumulated by severe deformation could activate recrystallization and thus control the austenite grain size and create an appropriate microstructure for the SME. The main objective was to find new ways to improve the SME of the alloy and to widen the spectrum of applications. In this paper, we analyse phases, texture, microstructure, critical temperatures and mechanical and shape memory properties of the material after one ECAE pass. In addition we examined the effect of annealing temperature.

2. Materials and methods

The Fe-15Mn-5Si-9Cr-5Ni nominal composition alloy was prepared in an induction furnace operating at 10 KHz and 30 KW. This material shows a very low SFE, between 5 mJ/m^2 [17] and 12 mJ/m^2 [18], according to different authors. Commercial raw material was melted in a high-purity alumina crucible under a protective argon atmosphere and cast into rectangular sand moulds. The ingots were homogenized at 1150 °C for 3 h to eliminate segregation defects. The ECAE samples were machined into a billet 600 mm long with a 7 mm square cross section. A well lubricated sample was fed into the input channel at 250 °C and pressed with a punch to the output channel. The interception angle, extrusion velocity, and maximum load were 120°, 5 mm/min, and 40 kN, respectively. Fig. 1 shows the ECAE block as prepared for the extrusion (a), and after the deformation was interrupted (b). The nondeformed portion represents the as-cast condition of the material and is useful for comparison purposes. Several samples were obtained from this billet, as shown in Fig. 2. One belongs to the nondeformed condition (**ND**). We cut five samples from the deformed portion. One sample was left as extruded (**ED**) and the others were annealed at 800, 900, 950 and 1000 °C. They were identified as **E8**, **E9**, **E95** and **E10**, respectively.

For characterization, samples were first mechanically and then electrolytically polished in an 80/20 solution (vol.%) of acetic/perchloric acid at room temperature and 27 V. Diffractograms and XRD inverse pole figures were measured using Cu-Kα_1/Kα_2 lines in a Philips X-pert pro MPD goniometer. The initial data was corrected for defocusing and further analysed by WXpopLA (the current Windows 7 implementation of the popLA software) [19]. The martensitic transformation was activated by compression in an Instron 3362 universal testing machine, fixtured as shown in Fig. 3. The quantity of martensite was determined by the Rietveld method, as implemented in the MAUD program (Material Analysis Using Diffraction http://maud.radiographema.com/). This method allows for the incorporation of the full texture, or preferred orientation, analysis into the traditional refinement. The reverse transformation was activated in an in-house manufactured dilatometer, by

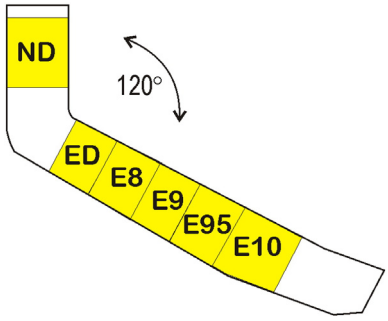

Fig. 2. The locations of samples taken from the ECAE billet.

Fig. 3. A sample being compressed. The image shows how the extensometer was attached to measure the deformation.

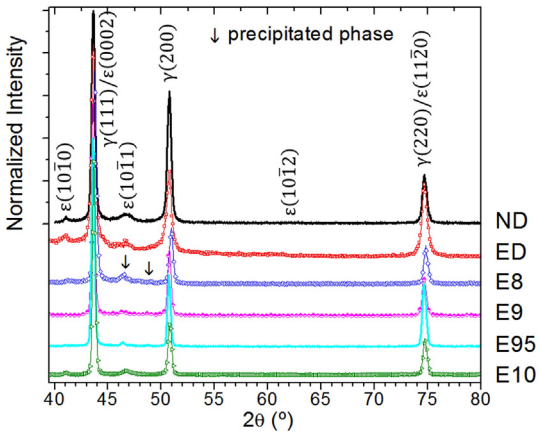

Fig. 4. X-ray patterns obtained from the mid-thickness of all samples. The planes and phases are identified by Greek symbols followed by the Miller indices (*hkl*).

heating the specimens to 400 °C, which is above the A_f temperature. Direct and reverse transformation temperatures were measured in these tests. The degree of uniaxial shape recovery (DSR_u) was calculated as:

$$DSR_u = \frac{l_2 - l_1}{l_1 - l_0} \cdot 100$$

where, l_0, l_1 and l_2 are the initial sample length, the length after compression and the length after reverse transformation, respectively.

Microstructural analyses were performed using a PME3 Olympus optical microscope (OM) equipped with a Nomarsky interference contrast device and a Philips CM200 transmission electron microscope with an acceleration voltage of 200 kV and an ultra-twin objective lens. After the electrolytic polish, OM samples were etched with Villela's reagent and a mixture of 10 ml HNO_3, 10 ml acetic acid, 15 ml HCl and 2 drops of glycerol. TEM foils were prepared from 0.2 mm thick discs, which were thinned by the double jet technique using a 95/5 vol.% solution of acetic and perchloric acids at room temperature.

3. Results

3.1. Shear deformation, X-ray diffraction and textures

Shear strain is uniform throughout the extruded ECAE billet, which allows one to determine distortion of structural elements such as grains and phases at each point. Segal's analysis [20] shows that punch pressure (p) and the increment of strain intensity ($\Delta\epsilon_i$) that the material experiences when passing through the shear plane are functions of the angle (2ϕ) between the channels and the flow stress of the material (Y):

$$\frac{p}{Y} = \Delta\epsilon_i = \frac{2}{3^{1/2}}\cot\Phi$$

The calculated values of punch pressure to flow stress ratio (p/Y) and the incremental strain intensity ($\Delta\epsilon_i$) for $2\phi = 120°$ are both 0.68. The reduction ratio (RR) and area reduction (AR) for equivalent "ideal" forming operations accomplished by a change of billet cross-sectional area from F_o to F are

$$RR = \frac{F}{F_0} = \exp\Delta\epsilon_i = 1.95$$
$$AR = \left(1 - RR^{-1}\right)100 = 49\%$$

The ECAE deformation pass develops different structures and textures in the material. XRD patterns obtained from the mid-thickness of the samples are shown in Fig. 4. Each phase is identified by its traditional Greek symbol, followed by the Miller indices (*hkl*) of the corresponding set of planes satisfying the diffraction condition. The symbol ↓ identifies a precipitate-phase that will be analysed thereafter. All the samples exhibited principally austenitic peaks, but low intensity ε peaks were also detected in the nondeformed (**ND**), single pass 120° channel (**ED**), 800 °C annealed (**E8**), 950 °C annealed (**E95**) and 1000 °C annealed (**E10**) samples. It is thought that thermal ε-martensite (ε_t) and stress induced martensite ($\varepsilon_{SI\ ecae}$) formed in the as-cast material and during the extrusion, respectively. Maji et al. [21] measured the martensite start temperature (Ms) for this alloy and found values above room temperature when austenitic grains are large and free of dislocations. The ε-martensite volume fractions are 9, 18, 7.6, 5.9 and 10.8% for **ND**, **ED**, **E8**, **E95** and **E10 samples**, respectively (see Table 1).

Texture development was investigated by measuring the {111}, {101} and {200} pole figures of the FCC phase. Fig. 5a, b and c show the inverse pole figures of the **ND**, **ED** and **E10** samples, respectively. The nondeformed material has a quasi-random distribution of crystallographic orientations (the shaded area in the normal direction (ND) figure should be considered an artefact. It is probably a consequence of large grain size). On the other hand after ECAE deformation, the material shows a larger near ⟨101⟩ component in the extrusion direction, which means the alloy is becoming textured. It is important to clarify that the ⟨101⟩ component is just 10° apart from ⟨414⟩, which is beneficial for a good SME, as we explain in the Introduction. Annealing does not substantially modify the texture, as can be observed in Fig. 5c. That particular sample was heated to 1000 °C and is the most heavily recrystallized. The spotty appearance of the texture in the **ED** material is characteristic of a large grain size. In contrast, in the recrystallized sample, the smoothness of the texture is typical of a fine grain size material.

3.2. Shape memory behaviour

To induce the γ → ε martensitic transformation, we compressed the samples in an Instron universal testing machine. The applied deformation was measured with an extensometer fixed in the manner shown in Fig. 5, and data from these measurements are given in Table 1. The

Table 1
Percent of ε-martensite before compression, stress that induces permanent deformation ($\sigma_{0.2}$), percent of compressive deformation (∈), percent of total ε-martensite after compression, percent of ε-martensite induced by the compression, degree of shape recovery (DSR), and average grain size for all samples.

Sample	Quantity of ε-martensite before the compression test (%)	$\sigma_{0.2}$ (MPa)	∈ (%)	Total ε-martensite after the compression test (%)	ε-Martensite induced by the compression test (%)	DSR (%)	Average grain size (μm)
ND	9 (ε_t)	430	2.3	16	7	47.8	290
ED	18 ($\varepsilon_t + \varepsilon_{SI\ ecae}$)	620	2.3	20	2	20.0	210
E8	7.6 (remnant of $\varepsilon_t + \varepsilon_{SI\ ecae}$)	600	2.0	15	7.4	27.7	208
E9	0	570	2.3	14	14	40.0	18
E95	5.9	530	2.7	17.5	11.6	51.3	26
E10	10.8 (ε_t)	430	2.3	20	9.2	63.6	53

σ-ε curves in Fig. 6 show the different behaviours of each sample. The yield stress was determined by the 0.2% offset method. Depending on the M_d value, the permanent deformation may be due to the $\gamma \rightarrow \varepsilon$ martensitic transformation ($\sigma_{\gamma \rightarrow \varepsilon}$) and/or to perfect dislocation glide (σ_y). The $\sigma_{0.2}$ of the nondeformed and extruded materials (Fig. 6a) are 430 and 620 MPa, respectively, which indicates that the alloy experienced extensive hardening when passed through the extrusion channel. The annealed samples (Fig. 6b) had activation stress values between those cited above, as is summarized in Table 1. These compressive stresses are in agreement with Bernardi et al. [7], although they found lower values for the softer conditions. The total fraction of ε-martensite after the compression tests was determined by refinement of the diffractograms shown in Fig. 7. These results are also summarized in Table 1. To account for the fact that samples contained ε-martensite before the test, the quantities induced by the compression were calculated as the difference in ε-martensite before and after testing. The martensite lathes introduced during testing might be, in principle, the only ones contributing to the SME after the reverse transformation.

The reverse transformation was activated by heating the samples to 400 °C in a dilatometer and the DSR was calculated as indicated in Section 2. There was a great deal of scatter in these results, as Table 1 shows. This will be discussed later.

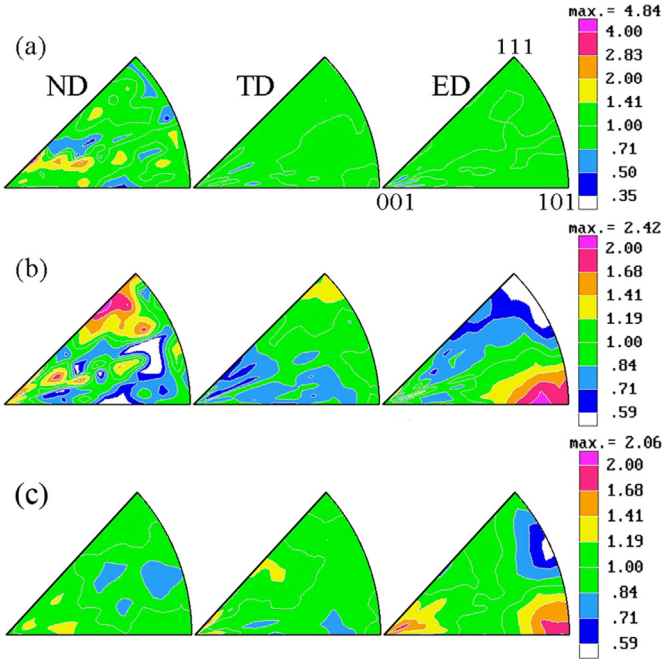

Fig. 5. Inverse pole figures of the nondeformed (a) extruded (b) and 1000 °C annealed (c) material. In this figure, ND, TD and ED indicate the normal, transverse and extruded directions, respectively.

3.3. Critical temperatures

The reverse transformation activates during heating when the driving force reaches a given value, called resistance-to-start-the-transformation energy (RSTE) [22]. A high As temperature means that the driving force needed to start the $\varepsilon \rightarrow \gamma$ transformation is also high. To determine the effect of ECAE and subsequent annealing on the As and Af temperatures, we heated the compressed samples in a dilatometer.

Fig. 8 shows the dilatometry curves and the graphical procedure to obtain the $\varepsilon \rightarrow \gamma$ reverse transformation start and finish temperatures. Regrettably, the martensite start temperature, Ms, could not be determined during cooling because the associated inflection is not well marked in the curves. Fig. 9 shows the results. The sample annealed at 900 °C, **E9**, shows the lowest As and Af values among all the conditions, 60 °C and 260 °C respectively. These values are significantly lower than those of the alloy annealed at 800 °C and 1000 °C. In these cases, the critical temperatures are similar, although the behaviour is due to very different microstructural conditions, as we will analyse later. On the other hand, comparing the temperatures for the as-cast and ECAE deformed alloys one can suppose that the material has accumulated sufficient energy to increase the reverse martensitic transformation temperatures.

3.4. Microstructural analysis

OM observations permit the characterization of the grain size and morphology, and they are important data for explaining the material behaviour. Fig. 10 displays four optical micrographs, and Table 1 summarizes the average grain size for all the conditions. Grain Size values were determined by the linear-intercept method using the ImageJ software. The structure of the nondeformed material, shown in Fig. 10a, consists of coarse austenite grains with an average grain size of around 290 μm. Extrusion deformation did not completely break down the solidification structure, as can be observed in Fig. 10b, a low magnification image of an **ED** sample after 2.3% compression. In this case, the average grain size is 210 μm, and stress induced ε-martensite (ε_{SI}) appears as curved streaks on the specimen surface. The appearance is similar to that reported by Bergeon et al. [23]. They found that the surface of stressed specimens had many parallel striations, certainly corresponding to the ε bands, whereas the surface topography of thermally treated samples remained smooth. Bernardi et al. [7] also found no significant grain refinement even after one ECAE pass and annealing at low temperatures. As can be deduced from Table 1, the cold-extruded structure persists up to 800 °C, above which the recrystallization process starts. Fig. 10c shows a completely recrystallized structure of ~18 μm grains in the sample annealed at 900 °C. After annealing at 950 °C, the structure has 26 μm equiaxed austenite grains and annealing twins (Fig. 10d). The grains grew to 53 μm after the 30 min 1000 °C anneal.

We also performed TEM analysis to obtain fine microstructural details. The nondeformed (**ND**) material (Fig. 11a) has an austenitic matrix containing a high density of stacking faults (SFs) in three directions. The zone axis in Fig. 11 is $[011]_{FCC}$. At higher magnification, we observed SFs

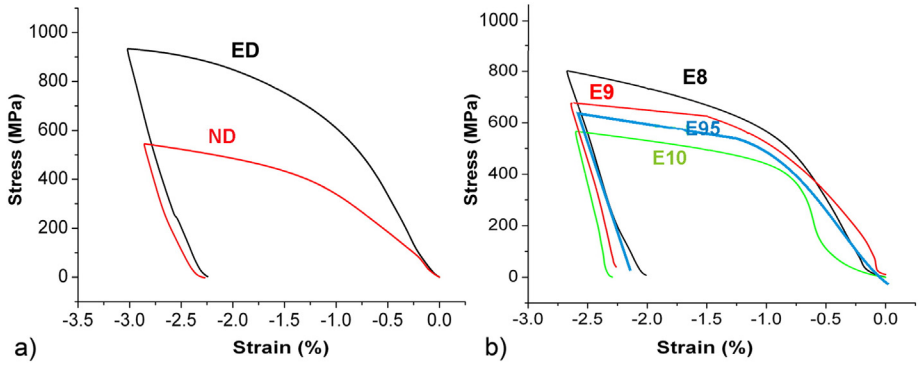

Fig. 6. Stress-strain curves obtained by compression: a) nondeformed (**ND**) and extruded (**ED**) samples; b) samples annealed at 800, 900, 950 and 1000 °C (**E8**, **E9**, **E95** and **E10**).

and some martensite plates (Fig. 11b). This is confirmed by the TEM dark field (DF) image shown in Fig. 11c.

As a consequence of the extrusion deformation, many defects and stress-induced ε-martensite plates formed. Fig. 12a shows a BF image of a typical area containing HCP martensite plates, in an almost edge-on condition. The zone axis is $[110]_{FCC}$ (see the SAD pattern inset on Fig. 12a). In this image, there are a high density of dislocations, SFs, and a dislocation band within an austenite matrix. Fig. 12b is a DF image taken using a martensite spot in the SAD pattern, so the plates appear in bright contrast. Other spots in the diffraction patterns confirm that various martensite variants were formed during the severe deformation.

TEM foils taken from sample **E8** show that the recrystallization process has already started at 800 °C. Some small, chain-like nuclei formed, probably in a former deformation band, as shown in Fig. 13a. They are recognized by the extra spots in the SAD pattern inset in the figure. Stacking faults can be seen in the nuclei interior, as a consequence of the alloy's low SFE. On the other hand, the austenitic matrix remains highly deformed and the number of SFs seems to have increased, probably due to dislocation dissociation during the recovery stage performed at 800 °C for 30 min. In addition, some second-phase particles precipitated at this annealing temperature. Fig. 13b shows an area with SFs, dislocations, and rounded particles lying in the deformed austenite.

Fig. 13c shows a single precipitate located at the edge of the foil perforation. The chemical composition of this precipitate and others similarly located were measured using TEM-EDS, and the results are summarized in Table 2. The compositional values are reliable due to the absence of matrix material contributions to the measurement. We recently investigated the structure of this second phase [24]. The Rietveld refinement of X-ray patterns, using the Maud software, indicates that the particles are compatible with a $Fe_5Ni_3Si_2$ type intermetallic phase, isostructural to the π-phase $Cr_3Ni_5Si_2$ with space group $P2_13$ and a lattice parameter equal to 0.6227(7) nm.

The ECAE sample annealed at 900 °C (**E9**) has a completely recrystallized structure. No dislocations but many SFs appear in the TEM image, see Fig. 14a. Fig. 14b shows that the SFs stop at the boundaries of the small grains.

Annealing at 950 °C reproduces the structure described above, although the grains have grown as indicated in Table 1. The low magnification image in Fig. 15a illustrates the straightness of the grain boundaries, typical of recrystallization. Fig. 15b shows SFs and an isolated thermal ε-martensite plate. Partial dislocations are observed at the beginning and the end of the SF in the centre of the image.

The structure after annealing at 1000 °C contains the same features as found in the samples annealed at 900 and 950 °C. Fig. 16a is a high magnification image where two {111} planes are seen in an almost edge-on condition, and stacking faults overlap on the $(\overline{1}11)$ planes. The zone axis is near [110]. The presence of martensite on the $(\overline{1}11)$ plane, indicates that the Ms. is above room temperature. The TEM dark field image, Fig. 16b, shows the martensite plate in bright contrast. It can be seen that the martensite plates are actually composed of a fine distribution of thin HCP plates.

4. Discussion

The nondeformed material shows a distribution of quasi-random crystallographic orientations. Thus, texture does not influence the martensitic transformation. The high density of SFs and the absence of perfect dislocations, see Fig. 11, facilitate permanent deformation, either by

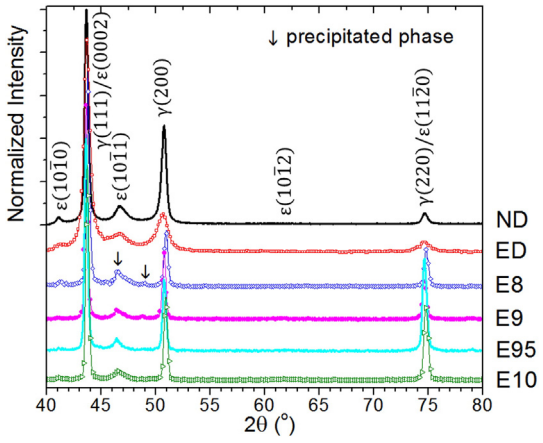

Fig. 7. X-ray patterns of the specimens after compression. The planes and phases are identified by Greek symbols followed by the Miller indices (*hkl*).

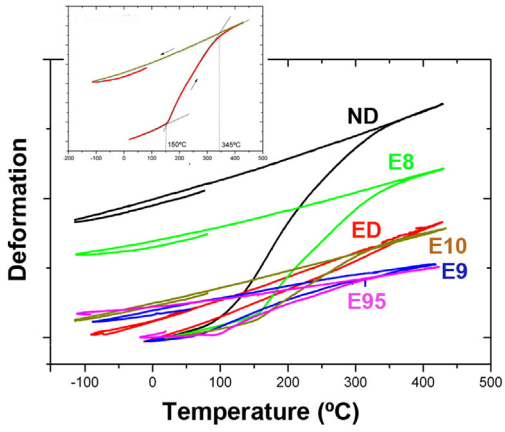

Fig. 8. Determination of the critical temperatures by dilatometry. The graphic method used to obtain the values shown in Fig. 9 is illustrated in the inset.

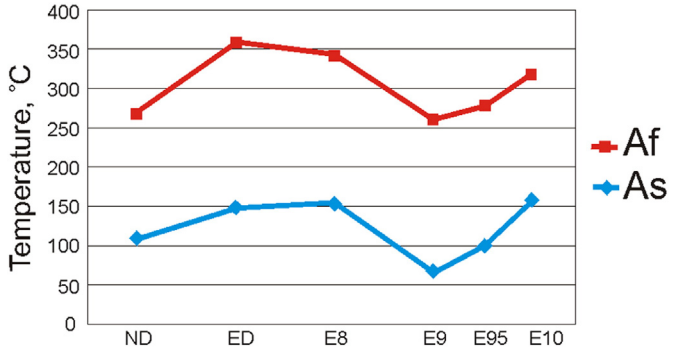

Fig. 9. As and Af reverse martensitic transformation temperatures, determined from the curves shown in Fig. 8.

activation of the γ → ε martensitic transformation or through deformation of the soft austenite during compression. In addition, having the matrix free of dislocations may ease the reverse transformation, as denoted by the low As value. The ε plates recover to austenite between 111 °C and 271 °C, the lowest Af temperature among the cases investigated. For this condition, the degree of shape recovery (<50%) can be attributed to the austenite softness. The matrix can thus undergo pure plastic deformation or simultaneously accommodate some γ → ε volume change, also by means of plasticity. This means that the current soft austenite cannot retain the elastic energy needed to activate the reverse transformation over the same path followed by the direct transformation. Thus, the reverse transformation must occur on another variant.

Although ECAE develops a texture favourable to the martensitic transformation, the effect of hardening due to cold working dominates the SME in the **ED** sample. The high value of $\sigma_{\gamma \rightarrow \varepsilon}$ indicates an increase of the resistance-to-start-the-transformation energy (RSTE), which retards the beginning of the movement of the partial dislocations. This phenomenon could be attributed to martensite nuclei retained by the local stress fields surrounding dislocation tangles in the matrix. In addition, the 18% of pre-existent martensite plates impede the development of only one transformation variant. As the γ → ε transformation starts at such a high stress, 620 MPa, many martensitic variants could activate simultaneously. The ε → γ reverse transformation critical temperatures also indicate a high RSTE. This can be rationalized since the HCP martensite transforms to FCC by coalescence of partial dislocations, and the presence of such a high number of crystallographic defects could obstruct, at least partially, their complete coalescence. The consequence of such a wrought matrix and prior martensite is the lowest DSR among all the cases. Other researchers [5–7] obtained similar results and performed subsequent annealing to recover and recrystallize the highly plastically strained structure.

How does annealing act? Obviously, its effect is related to the structural modifications produced at a given temperature. After annealing at 800 °C, the structure remains highly deformed, except for the sites of greatest energy accumulation where the nuclei for an incipient recrystallization are observed. Some martensite plates – which are not shown in the figures – continue to exist, despite annealing at a temperature above the measured Af (345 °C). This confirms the hypothesis that the high density of defects hinders the reverse transformation or, at least, renders it incomplete. The critical temperatures, the $\sigma_{0.2}$ stress, and the DSR of the annealed samples varied slightly when compared to the extruded alloy. The amount of martensite, indicated in Table 1

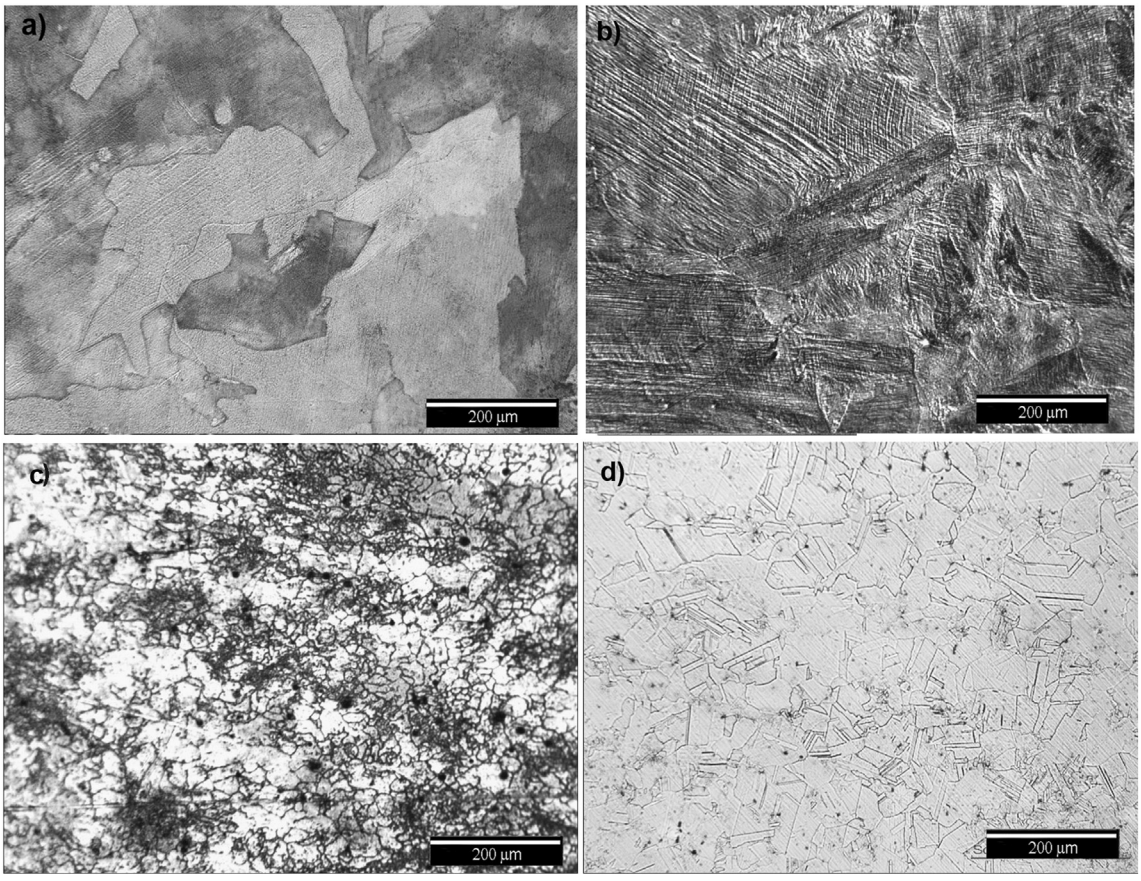

Fig. 10. Optical micrographs of (a) the nondeformed alloy, (b) an **ED** specimen after 2.3% compression (NIC), (c) the alloy extruded and annealed at 900 °C for 30 min, **E9**, and d) the extruded alloy after annealing at 950 °C, **E95**.

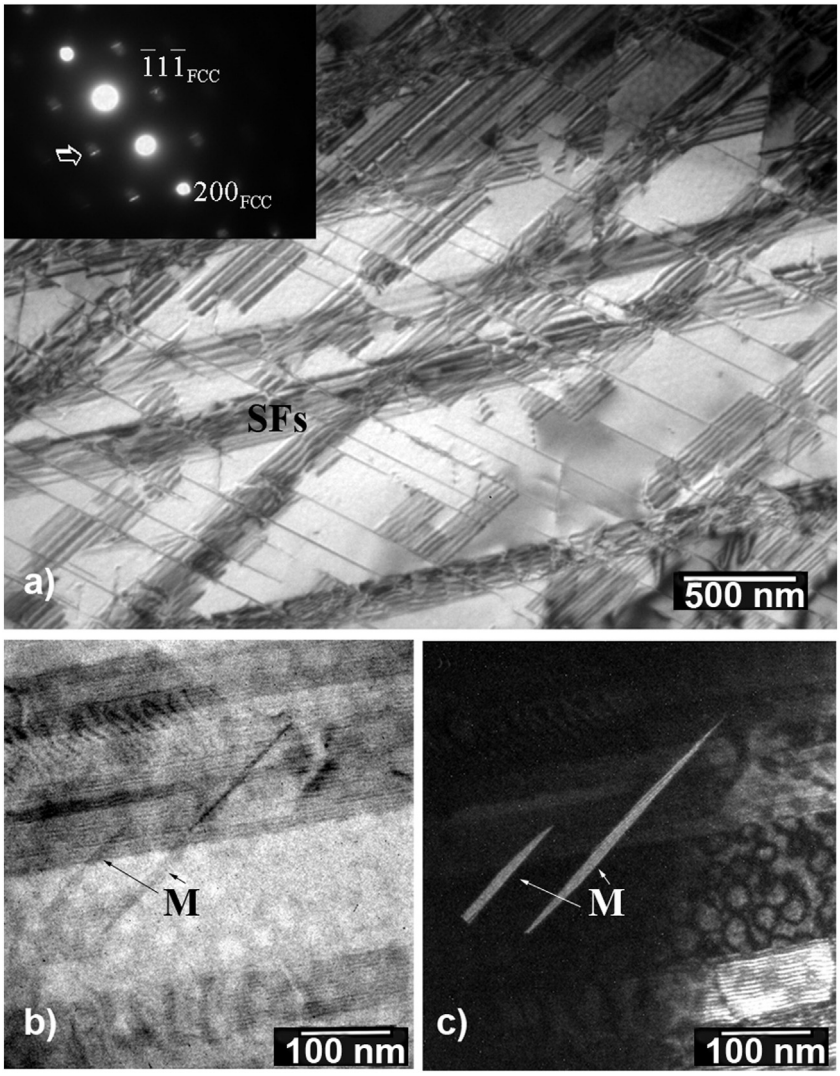

Fig. 11. TEM images taken from the **ND** as cast material. a) A bright field (BF) image that shows a white austenite matrix and a high density of stacking faults (SFs) in three directions. The inset shows the selected area diffraction (SAD) pattern. The zone axis is $[011]_{FCC}$. The bright streaks (see the arrow) in the SAD image indicate the presence of the SFs. b) This high magnification image contains SFs and thin parallel martensite plates (M). c) A DF image of the same area showing the martensite plates in bright contrast and differently oriented SFs.

for sample **E8**, is lower because some of what was induced by the extrusion reverts to austenite during the 800 °C annealing.

Heating at 900 °C produces a completely recrystallized structure and the shear texture (near ⟨414⟩// extrusion direction) remains after recrystallization, which is favourable for activation of the $\gamma \rightarrow \varepsilon$ induced martensitic transformation before plastic deformation. The grains are small, ~18 μm, due to extensive nucleation at the sites of high accumulated energy. Only SFs and precipitates lie in the austenitic matrix. This result agrees with Bernardi et al. [7] who observed a finely recrystallized austenite structure for both compositions (with and without Co). Also Maji et al. [25] found a recrystallization start temperature of about 850 °C in an alloy with a composition similar to ours. However, in other investigations by Zhang et al., material similar to ours but with higher Mn and deformed in two ECAE passes recrystallized at 600 °C [5] and 750 °C [6]. It is known that chemical composition and, overall, the accumulated deformation energy influences the recrystallization temperature. However, in the two papers by Zhang et al., the heating after pressing activates an aging process. The precipitation of chromium carbides affects the critical temperatures and all other behaviours of the alloy, including the SME.

When sample **E9** was subjected to compression to induce the martensitic transformation, the quantity of martensite and the shape recovery were larger than for sample **E8**, which was annealed at 800 °C. In the case of sample **E9**, all the ε-martensite was induced during compression. The high value of the stress to induce the $\gamma \rightarrow \varepsilon$ transformation, 570 MPa, can be attributed to constraints at the grain boundaries, and probably, various martensitic variants were induced simultaneously. In addition, elastic energy concentrates in the proximity of the grain boundaries, where the martensite plates stop, as the extremely low As temperature would suggest. This samples DSR was larger than for the alloy deformed by ECAE before (**ED**) and after the annealing at 800 °C (**E8**). However, the DSR value is lower than that measured by Zhang et al. [4–6]. They attribute their results to an increased matrix strength which blocked the plastic deformation. The small quantities of carbon in their alloys precipitate as $Cr_{23}C_6$ during annealing, elevating σ_y the stress needed for dislocation glide.

After annealing at 950 °C, recrystallized grains grew to ~26 μm, which approximates values measured by Bernardi et al. [7]. Controversially, they attributed their best shape recovery results to the grain size. Unfortunately, they do not support their conclusion with TEM observations and texture measurements because other microstructural features could have contributed to their SME results, e.g. SF density and texture intensity.

Finally, the samples annealed at 1000 °C (**E10**) showed the best shape memory behaviour for our alloy. Texture and microstructure are responsible for this result. The texture is quite similar to that observed

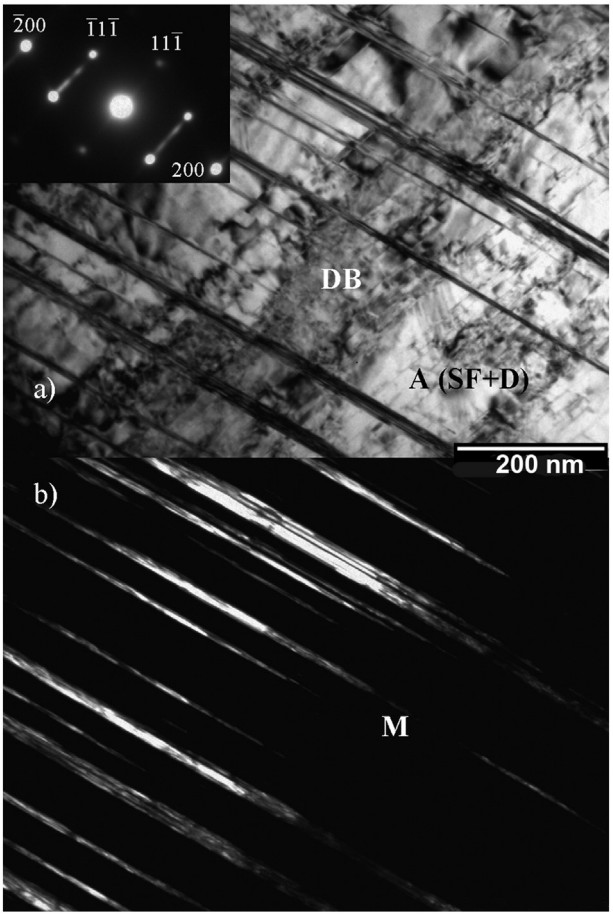

Fig. 12. TEM images of the deformed material, sample **ED**. a) A BF image showing stacking faults, a high density of dislocations and a deformation band (DB) in the center of the of the austenitic matrix. The zone axis is $[011]_{FCC}$. The bright streaks in the SAD pattern seem to be transforming to circles, which indicates that the black stripes are martensite. b) A DF image of the same area using one of the diffraction spots confirms the presence of martensite.

for samples **ED**, **E8** and **E9**, while the greatest differences between these samples lies in their microstructures. The short annealing time, 30 min, limited the grain growth to approximately 53 μm, much smaller than for samples **ND**, **ED** and **E8**. The high density of SFs could move freely, and consequently, martensite plates grew unhampered by either dislocation tangles (as in samples **ED** and **E8**) or by grain boundaries (as in sample **E9**, which had a slightly smaller grain size). On the other hand, sample **E10** with the larger grain size of the 53 μm seems to favour the growth of only one martensitic variant, in comparison to the **ND** sample. At the same time, the **E10** sample retains the necessary elastic energy to activate the reverse transformation over the same path followed by the direct transformation. The effects of the favourable texture and the grain size are evident since the $\gamma \rightarrow \varepsilon$ martensitic transformation was induced at low stress (430 MPa) and a large percentage of martensite was obtained (9.2%). This is very relevant because the permanent deformation initiated at the same stress as in the **ND** sample, where the grain size is much smaller than in sample **E10**. In samples **ND** and **E10** the kind and distribution of dislocations and SFs are similar, but the **ND** sample recovers far less of the imposed compressive permanent deformation. Under an applied stress, the mechanisms activated are different. Perfect dislocations glide in sample **ND** producing irreversible plastic deformation, while Shockley partial dislocation movement in sample **E10** activates the martensitic transformation. Consequently, the **E10** sample exhibited the best shape memory behaviour of all the cases studied, due to a favourable texture and adequate grain size.

Table 2
EDS determined chemical composition of the precipitate particles and the matrix corresponding to the **E8** sample.

Element	Particles	Matrix
Fe	61.9	64.7
Mn	18.2	17.5
Cr	10.4	10.1
Ni	5.1	4.6
Si	5.2	3.3

5. Conclusions

We investigated how severe deformation affects the properties of an Fe-15Mn-5Si-9Cr-5Ni (wt.%) SMA. The effects of phases, texture, microstructure, critical temperatures, mechanical and shape memory properties of the alloy were studied after one ECAE pass. In addition, microstructural changes as a function of annealing temperature were analysed. Our conclusions follow:

1. One ECAE pass introduced a shear texture, many dislocations and stress-induced ε-martensite. As a result, the stress $\sigma_{\gamma \rightarrow \varepsilon}$ to induce the $\gamma \rightarrow \varepsilon$ martensitic transformation was so high, 620 MPa, as to limit the quantity of ε-martensite formed after 2.3% compression. The critical temperatures to activate the reverse transformation, As and Af, of 50 and 90 °C respectively, were higher than those of the

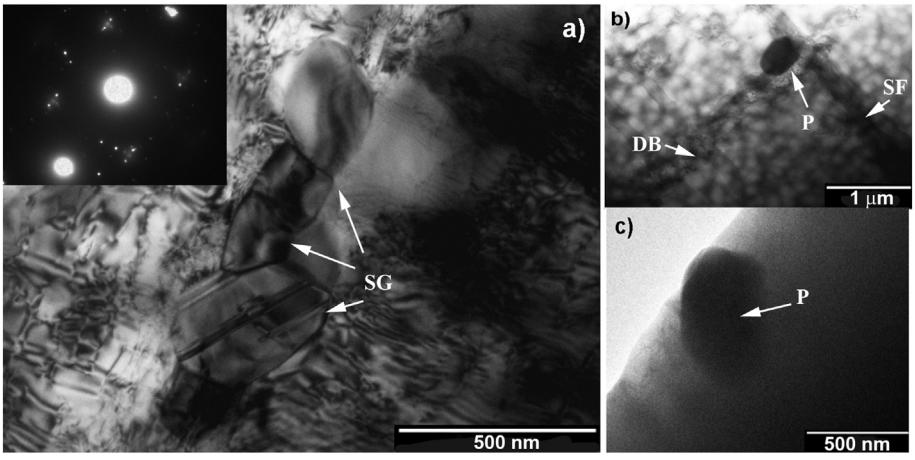

Fig. 13. BF TEM images of the deformed alloy after annealing at 800 °C, sample **E8**. a) Deformation bands (DB) and small recently nucleated grains (SG) in the austenitic matrix. The numerous spots in the diffraction pattern reflect all the grains (see inset). b) Precipitates (P), DB and SFs (zone axis [001]). c) A precipitate located just at the edge of the foil perforation.

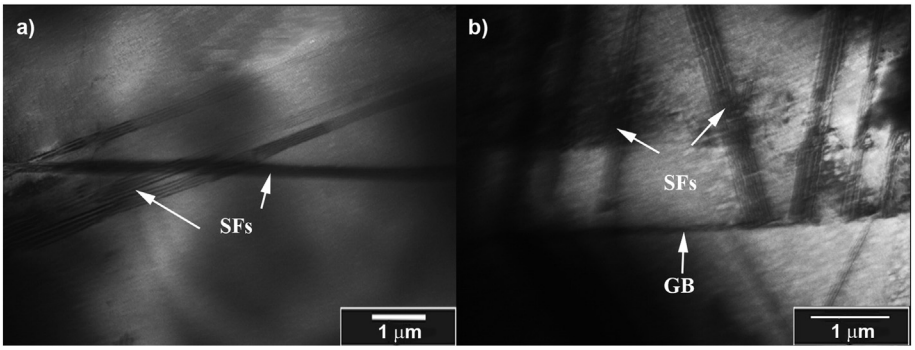

Fig. 14. BF TEM images of the deformed alloy after annealing at 900 °C, sample **E9**. a) In this image only SFs are visible in the austenitic matrix. b) SFs stopping at a grain boundary (GB).

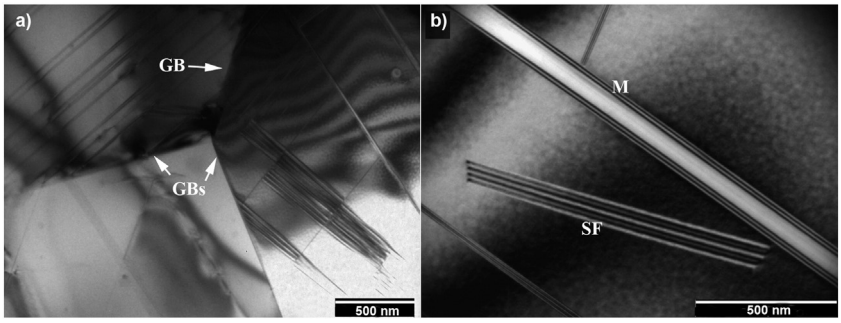

Fig. 15. BF TEM images of the deformed alloy after annealing at 950 °C, sample **E95**. a) Three austenite grains containing SFs that are stopped by the straight grain boundaries. (GB). b) An isolated martensite plate (M) and SFs in an austenitic matrix.

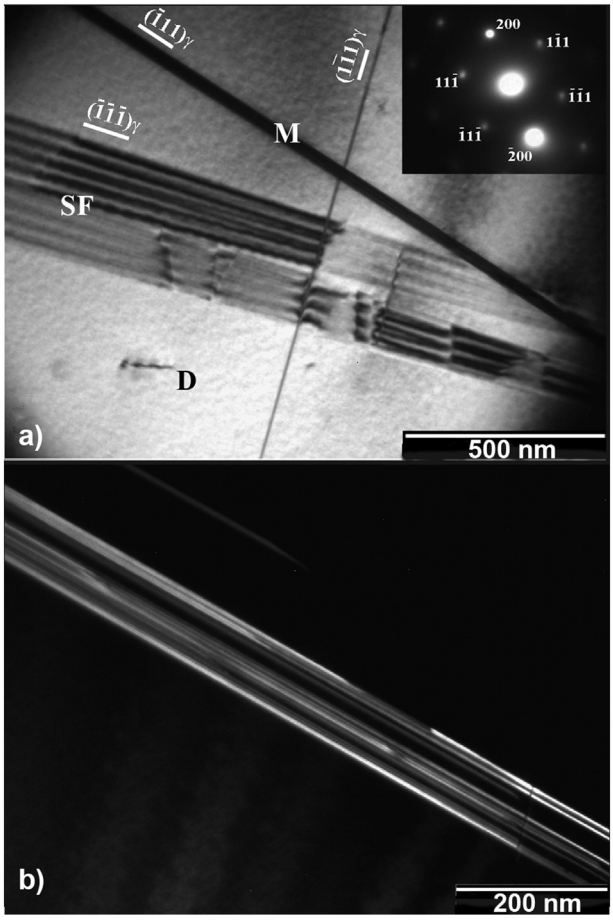

Fig. 16. TEM images of the deformed alloy after annealing at 1000 °C, sample **E10**. a) SFs on $(\bar{1}1\bar{1})$ and $(1\bar{1}1)$ planes, and a martensite plate on a $(\bar{1}11)$ plane. b) The DF image shows that martensite is formed as a fine distribution of plates. The zone axis is $[011]_{FCC}$.

nondeformed material and the degree of shape recovery was only 20%.

2. Subsequent heat treatments above 800 °C activated recrystallization yet the previously developed shear texture remained. The new grains had a high density of SFs and developed unique microstructural features: small nuclei after annealing at 800 °C; 18 μm grains appeared at 900 °C; and a grain size of 26 and 53 μm at 950 and 1000 °C, respectively. As annealing temperature is raised $\sigma_{\gamma \rightarrow \varepsilon}$ decreases and the quantity of induced martensite and DSR increases.
3. The samples extruded and annealed at 1000 °C achieved the best shape memory behaviour. The DSR was 64% and the stress to induce the martensitic transformation, $\sigma_{\gamma \rightarrow \varepsilon}$, was 430 MPa.

Finally, we wish to remark on some important concepts:

1) After ECAE deformation, high energy is stored in the material, such that the best final microstructure can be obtained by controlling the time/temperature parameters of the subsequent recrystallization.
2) The texture developed through ECAE deformation is favourable for the DSR since the material has a large ⟨101⟩ component, near the ideal ⟨414⟩, in the extrusion direction.

Acknowledgments

The authors thank Dr. H. Bernardi and Dr. K. Käfer for the ECAE processing in ITA, Brasil. We also thank Dr. M. Stout for proofreading this manuscript. Financial support from ANPCyT (PICT 1341), SecTyI-Prov. Santa Fe (2010-156-11) and SCyT-U.N.R. (PID ING255) is also gratefully acknowledged.

References

[1] A. Sato, E. Chishima, Y. Yamaji, T. Mori, Orientation and composition dependencies of shape memory effect in Fe-Mn-Si alloys, Acta Metall. 32 (4) (1984) 539–541, http://dx.doi.org/10.1016/0001-6160(84)90065-8.

[2] A. Druker, C. Sobrero, H.-G. Brokmeier, J. Malarría, R. Bolmaro, Texture evolution during thermomechanical treatments in Fe–Mn–Si shape memory alloys, Mater. Sci. Eng. A 481–482 (2008) 578–581, http://dx.doi.org/10.1016/j.msea.2006.10.214.
[3] V.M. Segal, V.I. Reznikov, A.E. Drobyshevski, V.I. Kopylov, Russ. Metall. (Engl. Transl.) 1 (1981) 99–105.
[4] W. Zhang, Y. Wen, N. Li, S. Huang, Remarkable improvement of recovery stress of Fe–Mn–Si shape memory alloy fabricated by equal channel angular pressing, Mater. Sci. Eng. A 454–455 (2007) 19–23, http://dx.doi.org/10.1016/j.msea.2006.10.101.
[5] W. Zhang, L. Jiang, N. Li, Y. Wen, Improvement of shape memory effect in an Fe–Mn–Si–Cr–Ni alloy fabricated by equal channel angular pressing, J. Mater. Process. Technol. 208 (2008) 130–134, http://dx.doi.org/10.1016/j.jmatprotec.2007.12.103.
[6] W. Zhang, L. Jiang, N. Li, Y. Wen, Microstructures and shape memory effect of different carbon-bearing FeMnSiCrNi alloys aged after Equal Channel angular pressing, Metall. Mater. Trans. B 38B (2007) 299, http://dx.doi.org/10.1007/s11663-007-9022-9.
[7] H. Bernardi, K. Käfer, L. Naito, J. Otubo, Shape recovery in stainless FeMnSiCrNi(−-Co) SMA processed by ECAE, Mater. Sci. Forum 738–739 (2013) 252–256, http://dx.doi.org/10.4028/www.scientific.net/MSF.738-739.252.
[8] S. Sajadifar, G.G. Yapici, Workability characteristics and mechanical behavior modeling of severely deformed pure titanium at high temperatures, Mater. Des. 53 (2014) 749–757, http://dx.doi.org/10.1016/j.matdes.2013.07.057.
[9] I. Puertas, C.J. Luis Pérez, D. Salcedo, J. León, J.P. Fuertes, R. Luri, Design and mechanical property analysis of AA1050 turbine blades manufactured by equal channel angular extrusion and isothermal forging, Mater. Des. 52 (2013) 774–784, http://dx.doi.org/10.1016/j.matdes.2013.05.089.
[10] S. Suwas, R. Massion, L.S. Tóth, J.J. Fundenberger, B. Beausir, Evolution of texture during equal channel angular extrusion of commercially pure aluminum: experiments and simulations, Mater. Sci. Eng. A 520 (2009) 134–146, http://dx.doi.org/10.1016/j.msea.2009.05.028.
[11] O. Higuera-Cobos, J. Berríos-Ortiz, J. Cabrera, Texture and fatigue behavior of ultrafine grained copper produced by ECAP, Mater. Sci. Eng. A 609 (2014) 273–282, http://dx.doi.org/10.1016/j.msea.2014.05.011.
[12] N.S. De Vincentis, A. Kliauga, M. Ferrante, M. Avalos, H.-G. Brokmeier, R.E. Bolmaro, Evaluation of microstructure anisotropy on room and medium temperature ECAP deformed F138 steel, Mater. Charact. 107 (2015) 98–111, http://dx.doi.org/10.1016/S1359-6462(01)00996-4.
[13] A. Druker, P. La Roca, P. Vermaut, P. Ochin, J. Malarría, Microstructure and shape memory properties of Fe-15Mn-5Si-9Cr-5Ni melt-spun ribbons, Mater. Sci. Eng. A 556 (2012) 936–945, http://dx.doi.org/10.1016/j.msea.2012.07.097.
[14] Volosevich et al. in. Y. Lee, C. Choi, Driving force for γ → ε martensitic transformation and stacking fault energy of γ in Fe-Mn binary system, Metall. Mater. Trans. A 31A (2000) 355.
[15] K. Bhattacharya, R.V. Kohn, Symmetry, texture and the recoverable strain of shape-memory polycrystals, Acta Mater. 44 (2) (1996) 529–542, http://dx.doi.org/10.1016/1359-6454(95)00198-0.
[16] G. Wang, H. Peng, P. Sun, S. Wang, Y. Wen, Effect of titanium addition on shape memory effect and recovery stress of training-free cast Fe–Mn–Si–Cr–Ni shape memory alloys, Mater. Sci. Eng. A 657 (2016) 339–346, http://dx.doi.org/10.1016/j.msea.2016.01.099.
[17] R. Xiong, H. Peng, S. Wang, H. Si, Y. Wen, Effect of stacking fault energy on work hardening behaviors in Fe–Mn–Si–C high manganese steels by varying silicon and carbon contents, Mater. Des. 85 (2015) 707–714, http://dx.doi.org/10.1016/j.matdes.2015.07.072.
[18] Y.H. Wen, H.B. Peng, D. Raabe, I. Gutierrez-Urrutia, J. Chen, Y.Y. Du, Large recovery strain in Fe-Mn-Si-based shape memory steels obtained by engineering annealing twin boundaries, Nat. Commun. 5 (2014) 4964, http://dx.doi.org/10.1038/ncomms5964 (|www.nature.com/naturecommunications).
[19] J. Kallend, U. Kocks, A. Rollett, H. Wenk, Operational texture analysis, Mater. Sci. Eng. A 132 (1991) 1–11, http://dx.doi.org/10.1016/0921-5093(91)90355-Q.
[20] V.M. Segal, Materials processing by simple shear, Mater. Sci. Eng. A 197 (1995) 157–164, http://dx.doi.org/10.1016/0921-5093(95)09705-8.
[21] B. Maji, M. Krishnan, The effect of microstructure on the shape recovery of a Fe–Mn–Si–Cr–Ni stainless steel shape memory alloy, Scr. Mater. 48 (2003) 71–77.
[22] A. Baruj, A. Fernández Guillermet, M. Sade, Effects of thermal cycling and plastic deformation upon the Gibbs energy barriers to martensitic transformation in Fe-Mn and Fe-Mn-Co alloys, Mater. Sci. Eng. A 273–275 (1999) 507–511, http://dx.doi.org/10.1016/j.jmatprotec.2007.12.103.
[23] N. Bergeon, G. Guenin, C. Esnouf, Characterization of the stress-induced o martensite in a Fe–Mn–Si–Cr–Ni shape memory alloy: microstructural observation at different scales, mechanism of formation and growth, Mater. Sci. Eng. A 238 (1997) 309–316, http://dx.doi.org/10.1016/S0921-5093(97)00458-9.
[24] V. Fuster, A.V. Druker, A. Baruj, J. Malarría, R. Bolmaro, Characterization of phases in an Fe–Mn–Si–Cr–Ni shape memory alloy processed by different thermomechanical methods, Mater. Charact. 109 (2015) 128–137, http://dx.doi.org/10.1016/j.matchar.2015.09.026.
[25] B. Maji, M. Krishnan, V. Hiwarkar, I. Samajdar, R.K. Ray, Development of texture and microstructure during cold rolling and annealing of a Fe-based shape memory alloy, JMEPEG 18 (2009) 588–593, http://dx.doi.org/10.1007/s11665-009-9428-4 (ASM International).